

Omnipulse test results

Don C. Lawton and Malcolm B. Bertram

ABSTRACT

A nine-component walkaway noise spread (32 geophones at 2 m intervals) was recorded with the Omnipulse™ source and 3-component geophones, to a maximum source receiver offset of 510 m. Matched source and receiver component data had the highest coherent energy level, with refractions, multiple refractions and surface waves being the major events recorded. Far-field P and S headwaves were found to have velocities of 3200 m/s and 1350 m/s respectively. Dispersive Rayleigh and Love waves were recorded, with group velocities less than 300 m/s and dominant frequencies of about 8 Hz. Love waves, generated with the SH source were particularly high in amplitude.

Post-acquisition array forming from the raw data showed a decrease in the relative amplitude and bandwidth of the surface wave energy. However, stacking resulted in severe phase distortion of these events.

Refraction analysis showed short-wavelength P-wave and S-wave statics of 5 ms and 15 ms over 4 m respectively, and a 5 degree standard deviation in apparent directivity.

INTRODUCTION

In the past 2 years, we have undertaken extensive field tests of 3-component geophones to determine their characteristics and fidelity (Lawton and Bertram, 1990, 1991). Generally, all of the cartesian 3-component geophones used in these experiments gave very similar results and all showed excellent decoupling between the 3 components (Vertical, Radial and Transverse).

Early in 1992, an opportunity arose to undertake additional field tests using multicomponent geophones and the Omnipulse source, a multicomponent seismic source which is capable of generating P, SH and SV waves at the same source location. The source is a modified Land Air Gun in which the ratio of vertical (P-wave) to horizontal (S-wave) energy produced can be varied by changing the angle of the pulse generator with respect to the base plate (Humphreys, 1989). A schematic diagram of the pulse generation unit of the Omnipulse is shown in Figure 1. When operated with the tower assembly in the vertical position, the unit performs as a conventional P-wave source. However, the tower assembly can also be rotated to an angle of 45 degrees from the vertical, in which case both P- and S-waves are generated simultaneously. In order to generate the equivalent of pure S-wave energy, two records are obtained with the tower assembly oriented in opposite inclinations, and the second record is then subtracted from the first. Note also that summing these two records provides the equivalent of a pure P-wave source. This subtraction and addition process to create equivalent pure S-wave and P-wave sources has been described previously by Hasbrouk (1987) and Lawton(1990).

OBJECTIVES

In production seismic profiling, normally 3 or 4 Omnipulse units are used synchronously. The source effort is increased further by vertically stacking several 'pops' at each source location. For the tests undertaken during this study, a single Omnipulse unit only was available, and a single 'pop' was recorded for each source orientation because of the absence of a stacking unit in the University's recording system. The objectives of the program were to:

- (a) Record and evaluate a full 9-component noise spread using the Omnipulse source;
- (b) Evaluate the near and far-field directivity response of 3-component geophones;
- (c) Evaluate receiver arrays versus point receivers for 3-component geophones;
- (c) Characterize the P- and S-wave velocity structure of glacial surface sediments and Tertiary bedrock typical of southern Alberta Plains and Foothills regions.

STUDY AREA

The experiments were conducted at the University of Calgary Farm at Spy Hill in Northwest Calgary (Twp 25, Rge 2W5). At this location, which is on the northwest extension of Nose Hill, the near-surface sediments consist of an unknown thickness of gravels and moraines deposited during the last glacial retreat. Bedrock consists of sandstones and shales of the Tertiary Paskapoo Formation.

DATA ACQUISITION

Data acquired for the study were collected over a 2-day period in March, 1992. The ground was unfrozen at the time of the survey and the weather was fine with only a slight breeze blowing from the southwest during recording. For all of the tests, a single receiver spread consisting of 32 single 3-component geophones was laid out in a north-south direction at the centre of the study area (Figure 2). A geophone separation of 2 m was used, and 2 geophones were clustered at the centre of the spread in order to create a total spread length of 60 m. Except for the 2 central geophones (provided by HGS and MP), OYO geophones were used and the horizontal components of the geophones were oriented with the reference arrows pointing in northerly (radial) and westerly (transverse) directions.

A total of 29 shot locations were occupied for the tests, with a distribution as shown in Figure 2. The source locations were grouped into 3 classes:

- (a) Noise spreads (Shotpoints 83 to 117)
- (b) Shot circle tests (Shotpoints C1 to C8)

(c) Near-field tests (Shotpoints N1 and S1).

At each source location, 4 separate records were obtained, with source modes of SH+, SH-, SV+, SV- respectively. For the SH mode, the tower assembly of the Omnipulse was tilted in a direction perpendicular to the source-receiver azimuth; for the SV mode, the tower was tilted in-line with the source-receiver azimuth. These different tilt directions for the SH and SV modes of operation required orienting the long axis of the truck to be in-line and cross-line with the source-receiver azimuth respectively.

For the noise-spread records, a source increment of 60 m was used (equivalent to a single spread length with an overlap of 1 geophone). Data were recorded north and south of the receiver spread, to a maximum offset of 510 m from the centre of the receiver spread. Due to access difficulties, there was some perpendicular offset required at many of the source points, particularly for those towards the north, as shown in Figure 2. Noise-spread data illustrated in this paper are restricted to the shotpoints south of the receiver spread.

Shotpoints C1 to C8 were located at 45 degree increments on a circle with a nominal radius of 200 m, although the actual distance at each shotpoint varied slightly because of local obstacles. Shotpoints N1 and S1 were located in-line with the receiver spread with near offset of 60 m.

A table of offset distances and azimuths of all shotpoints with respect to the centre and ends of the receiver spread are contained in Appendix 1.

All data for the study were recorded with a 96-trace Sercel 338B system using a 2 ms sampling interval and 3 second record length. No low-cut filters were used and the instruments were triggered with a time-break provided by the Omnipulse.

DATA PROCESSING

The initial step in processing consisted of sifting the data into common-component records. It was found that some traces were reversed in polarity and that the trace order of the HGS and MP geophones was different than that of the OYO geophones. These inconsistencies were corrected in the sift process.

Because only a single 'pop' was used for each record, there were some small differences in total energy between records obtained with the Omnipulse oriented in opposing tilt directions. In order to obtain the best separation between pure S and pure P source modes, the record pairs were balanced prior to subtraction and addition, respectively. Balancing was done on the basis of normalising the total absolute amplitude of the vertical component of each record pair. Output of this process consisted of suite of 9-component records, consisting of vertical (V), radial (R) and transverse (T) receiver components for each of the vertical (P), radial (SV) and transverse (SH) source modes.

In this paper, we provide the initial results from the noise-spread and near-field studies. Analysis of the shot-circle data is in progress.

RESULTS AND DISCUSSION

Noise spreads

Nine-component noise spread data are shown in Figures 3 to 11. Each figure consists of records from shotpoints 101 to 117 displayed adjacently in a single panel. For visual reasons, only every second trace of each data set is displayed, and agc scaling with a 0.75 s window length has been applied prior to plotting. The order of display are the V, R and T components for the P source mode (Figures 3 to 5, respectively), followed by the SV source mode (Figures 6 to 8, respectively) and then the SH source mode (Figures 9 to 12, respectively).

Figure 3 (P-V) shows a clear P-wave headwave arrival with an apparent velocity of 3200 m/s. This first arrival is followed by multiple refractions and then a dispersive Raleigh wave which has an average group velocity of about 280 m/s. The discontinuities in the surface wave events are due to the slight overlap in offset range for each record, and also must be related to changes in near-surface conditions local to each source location. No coherent energy is visible on the records after about 2 seconds. Figure 4 (P-R) has similar character to Figure 3 and shows a surprisingly coherent headwave arrival. However, this is not a pure P event since it is delayed by about 40 ms with respect to the P headwave arrival on Figure 3. We conclude that the first arrival in Figure 4 is a P-P-S refraction. The Raleigh wave recorded in Figure 4 has similar character to Figure 3, as expected. Figure 5 (P-T) shows weak P and S head-wave events leaking into the transverse receiver component, followed by multiples. Some of this energy is due to the source being located slightly off-line from azimuth of the receiver spread, although this is very small for the far offset source positions. The low-velocity, low-frequency event later in the record is interpreted to be Love wave energy.

Figure 6 (SV-V) is similar in character to the reciprocal (P-R) record (Figure 4). There is a weak P headwave arrival and also what is interpreted to be a weak S headwave (or an S-S-P refraction). Rayleigh waves very similar to those described on the P-V record (Figure 3) are observed. In the matched SV-R record (Figure 7), there is a very weak P headwave leaking into the radial component, followed by an SV headwave with an apparent velocity of 1000 m/s. Later events are multiple S-wave refracted arrivals and low frequency (8 Hz) Rayleigh waves. In Figure 8 (SV-T), the signal level is much lower than the matched components, as expected, as indicated by the amplified background noise. Weak refractions as well as some Love wave and Raleigh wave energy are observed in the data.

The final 3 noise records (Figures 9 to 11) were all recorded with an SH source mode. The highest coherent energy level is observed in Figure 11, which has matched source and receiver excitation directions (SH-T). These data show a very clear SH refracted headwave, with an apparent velocity of 1350 m/s. This event is followed by multiple refractions, then a very high-amplitude Love wave with a dominant frequency of 8 Hz, a group velocity of approximately 200 m/s and phase velocities between 250 and 350 m/s. This event is significant in that its high relative energy level could be problematic in SH reflection surveys. For the unmatched component (SH-R) data, shown in Figure 10, the SH headwave has a higher amplitude than expected. This may be due to offset source locations, or it may be an indicator of weak anisotropy in the weathering layer. Further analysis of these data will include receiver rotation to evaluate possible anisotropy. The remaining record (SH-R) contains weak S headwave events and elements of both Love and Rayleigh waves.

Near-field tests

Shotpoints N1 and S1 (Figure 2) were occupied in order to obtain data from near locations which were directly in-line with the receiver spread. The objective was to obtain a measure of the near-field purity of the source. Because of the limited energy available with only a single Omnipulse unit, and the lack of vertical stacking, a near offset of 60 m was used for this part of the study. This allowed data with a high signal to noise ratio to be obtained.

The data from N1 and S1 were processed in the same manner as the noise-spread data, and the 9-component data from shotpoint N1 are illustrated in Figure 12. Of significance in this figure is that all records are true relative amplitude, being scaled only by a time and offset invariant multiplier for plotting purpose. The records in Figure 12 show highest energy along the diagonal of the 9-component matrix, as expected for matched source and receiver excitation directions. In the off-diagonal records, there is very little coupling between SH source and either the V or R receiver components. Similarly, there is very little coupling between the P or SV source modes and the T receiver component. The highest coherent energy level in the off-diagonal records is recorded in the P-R and SV-V source-receiver data, and is interpreted to be caused by P-SV and SV-P mode conversions.

Array tests

The noise spread data enabled receiver arrays to be simulated from the raw field data. A subset of 17 traces from the receiver spread was selected for the array-forming tests as this distance (32 m) is typical of the geophone group length used on reflection surveys in western Canada. Figure 13 shows raw and stacked data from 3 records obtained from shotpoint N1. In order from top to bottom, these records are P-V, SH-T and P-R respectively. The traces on the left hand side of Figure 13 are derived from stacking various traces extracted from the raw data displayed on the right hand side of the figure. In the left panel, trace 1 is actually a single trace from the centre of the 17 receiver traces (i.e. trace 9); trace 2 is a stack of every fourth trace; trace 3 is a stack of every second trace, and trace 4 is a stack of all 17 traces of the input record. The stacked data have been trace-balanced prior to display. Amplitude spectra of the centre trace and each of the 3 stacked traces are shown for the 3 input panels in Figures 14, 15 and 16 respectively. Generally, array-forming narrows the bandwidth of the surface-wave energy and the array length is the critical parameter rather than the number of elements in the array. All arrays show a modest increase in the relative amplitude of the higher frequency (> 30 Hz) components of the first arrivals with respect to the amplitude of the surface waves. However, the data in Figure 13 show significant phase distortion of the surface waves after stacking, and indicates that the use of geophone groups may hinder the application of polarization filters to attenuate these events.

Array statics

The first arrivals across all 32 individual geophones in the receiver spread were picked for the P-V and SH-T records obtained from shotpoints N1 and S1. Reciprocal analysis of these data showed that the P-wave velocity is 2000 m/s and the SH-wave velocity is 1311 m/s, resulting in $V_p/V_s = 1.5$. Trace-to-trace P-wave and S-wave static variations across the spread were evaluated by refraction analysis and yielded a maximum difference (over 4 m) of 5 ms and 15 ms respectively. These values show that variations in statics across a group will cause some degradation of high frequency events.

Receiver directivity

Trace to trace directivity variations were studied by examining the first arrival energy azimuth at each geophone for an SV source located at shotpoint N1, which is at an azimuth of 0 degrees with respect to the radial component of the receiver spread. Figure 17 shows hodogram displays for the near and far geophones of the receiver spread. The analysis window is picked interactively and the maximum energy direction within that window for the 2 horizontal components is computed. Results from all geophones gave a mean azimuth of -2 degrees and a standard deviation of 5 degrees.

CONCLUSIONS

The following conclusions are drawn from the work completed at this time:

- (a) The Omnipulse displays excellent separation between P and S source-generated energy
- (b) A single 'pop' from a single Omnipulse generates useable data to offsets of about 500 m
- (c) A nine-component walk-away noise spread was successfully recorded. Good P and S headwave first arrivals were recorded in these tests. Love waves on the SH-T record had the highest amplitudes of all events recorded
- (d) Array forming showed some increase in the relative energy levels between headwaves and surface waves and a decrease in the bandwidth of surface waves. However, the array stack results in severe phase distortion of surface waves, which may hinder the effectiveness of polarization filters
- (e) In this location, short-wavelength static variations ranged up to 5 ms over 4 m for P-waves, and up to 15 ms over 4 m for S-waves
- (f) Near-field directivity response of the 3-component geophones was found to have a standard deviation of about 5 degrees.

ACKNOWLEDGMENTS

Bolt Technology Corporation kindly provided the Omnipulse source for these tests, and we acknowledge with thanks the assistance given to us by Stan Starzyck of Ref Tek Canada. We are also grateful to many CREWES Project staff members who provided willing help during the acquisition of the data, and to Dave Harvey and Carl Gunhold for the surveying of the shotpoints.

REFERENCES

- Hasbrouk, W.P., 1987, Hammer-impact, shear-wave studies; in Danbom, S.H. and Domenico, S.N., Eds., Shear-wave exploration: Geophysical Development Series, Vol 1, Soc. Expl. Geophys., 97-121.
- Humphreys, R., 1989, The omnipulse seismic source: Abstracts, SEG Research Workshop on Vector Wavefields, Snowbird, Utah, 47-48.
- Lawton, D.C., 1990, A nine-component refraction seismic experiment: Can. Jour. Expl. Geophys., 26, 716.
- Lawton, D.C. and Bertram, M.B., 1990, Field tests of 3-component geophones: CREWES Project Research Report, v. 2, 1-17.
- Lawton, D.C. and Bertram, M.B., 1991, Field tests of 3-component geophones, Part II: CREWES Project Research Report, v. 3, 1-27.

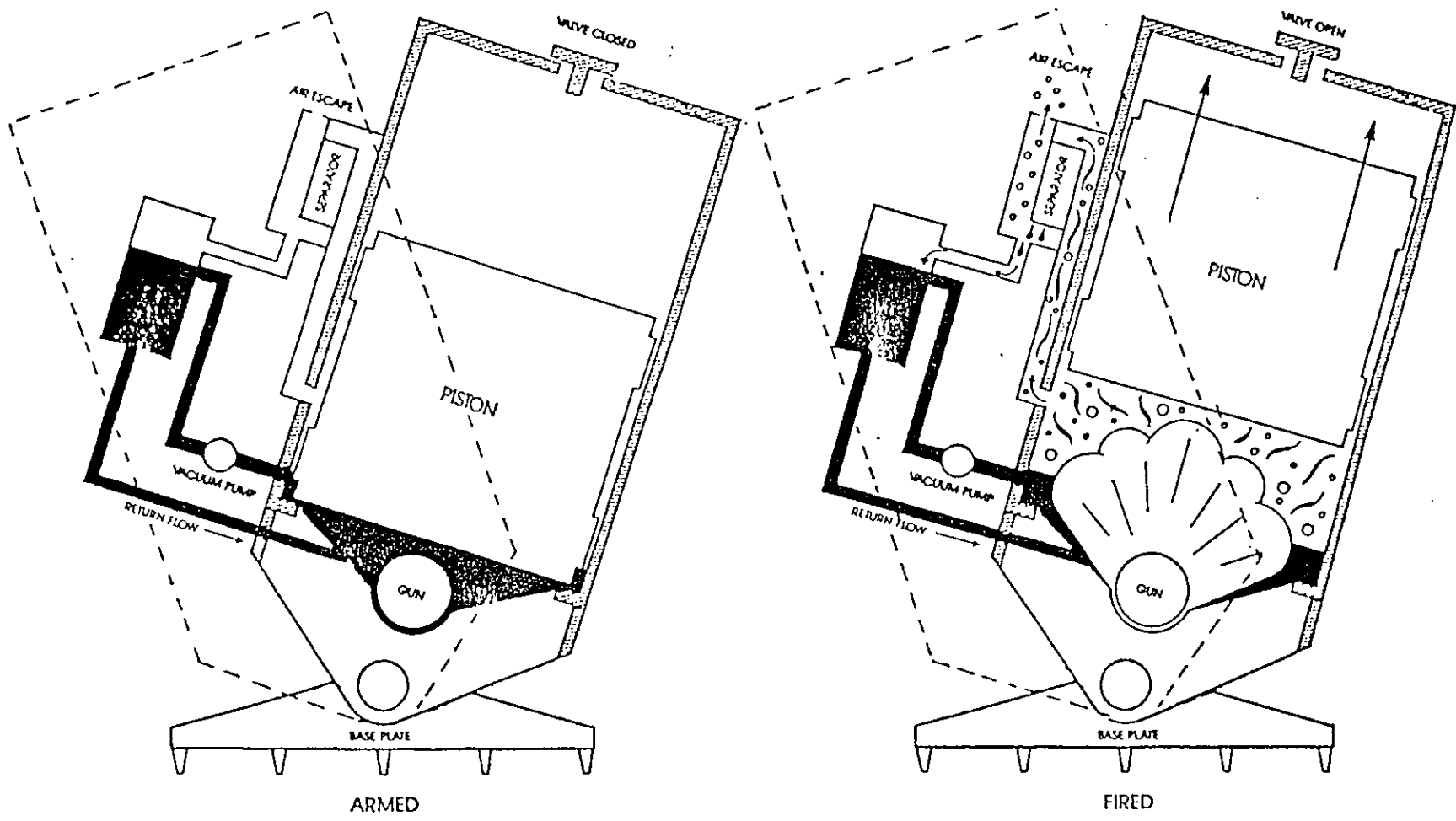


FIG. 1. Schematic diagram of the Omnipulse™ pulse generator (from Humphreys, 1989)

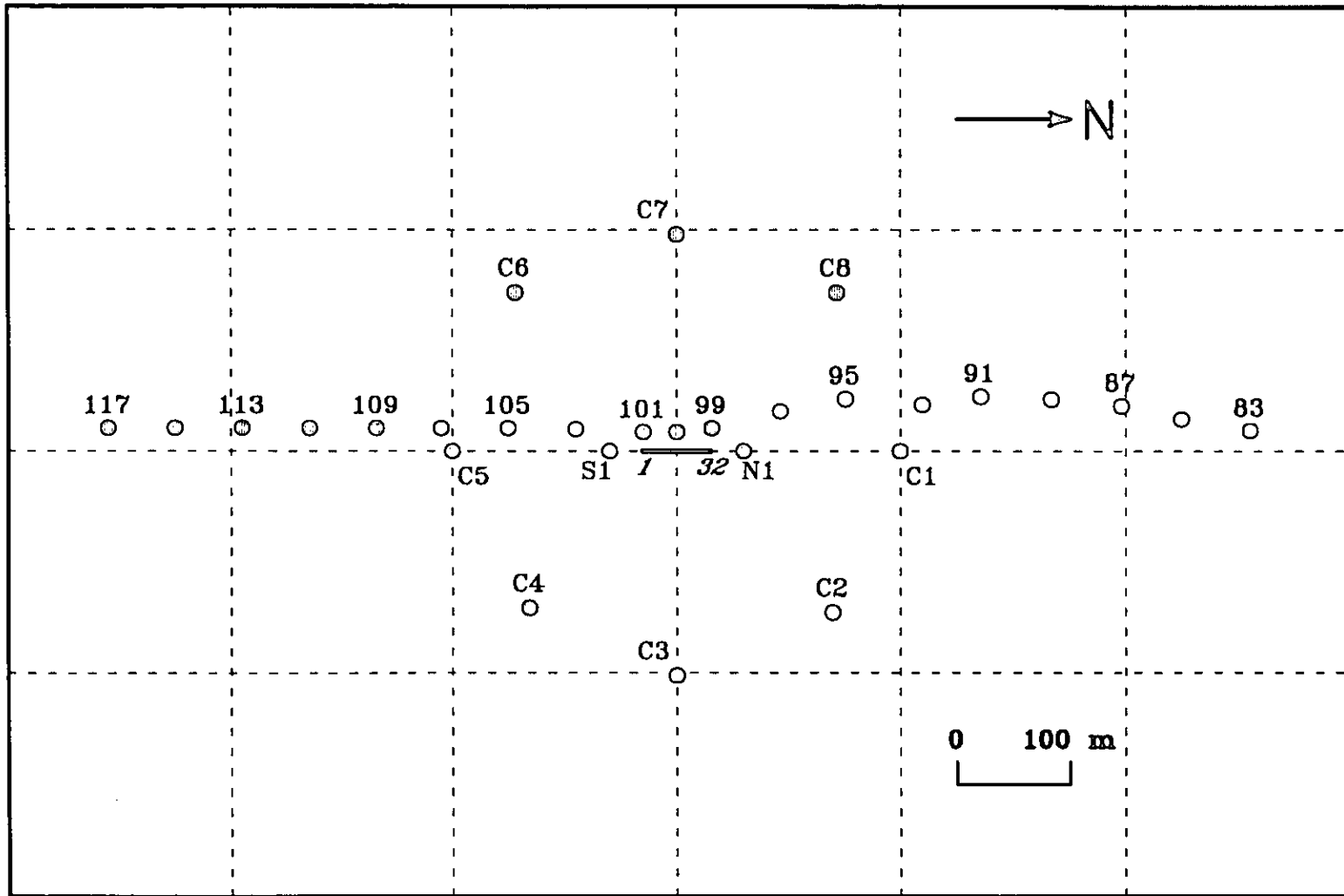
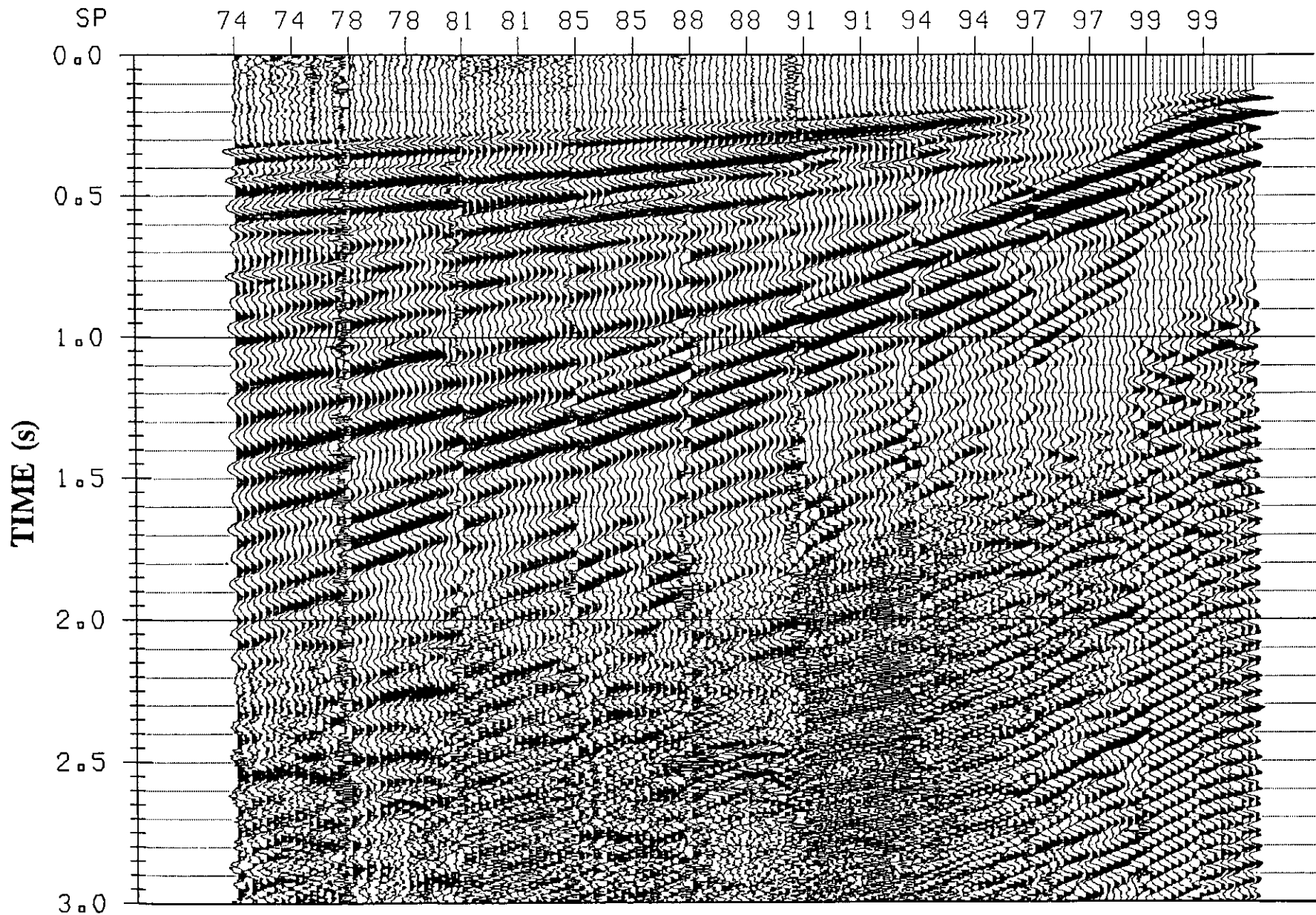


FIG. 2. Layout of shotpoints and receiver spread



Lawton, Bertram

FIG. 3. P-V noise spread data, shotpoints 101 to 117 (every second trace)

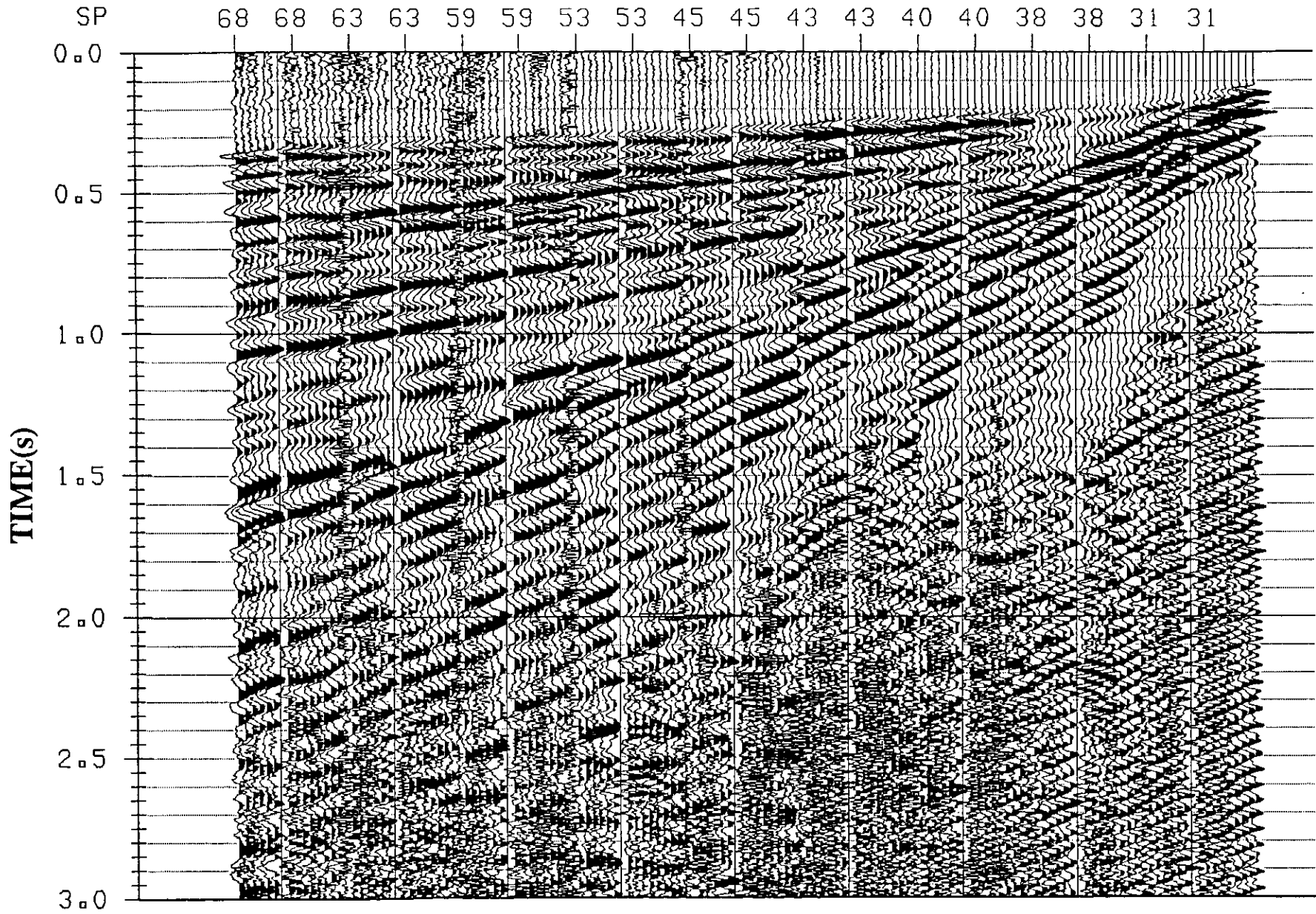


FIG. 4. P-R noise spread data, shotpoints 101 to 117 (every second trace)

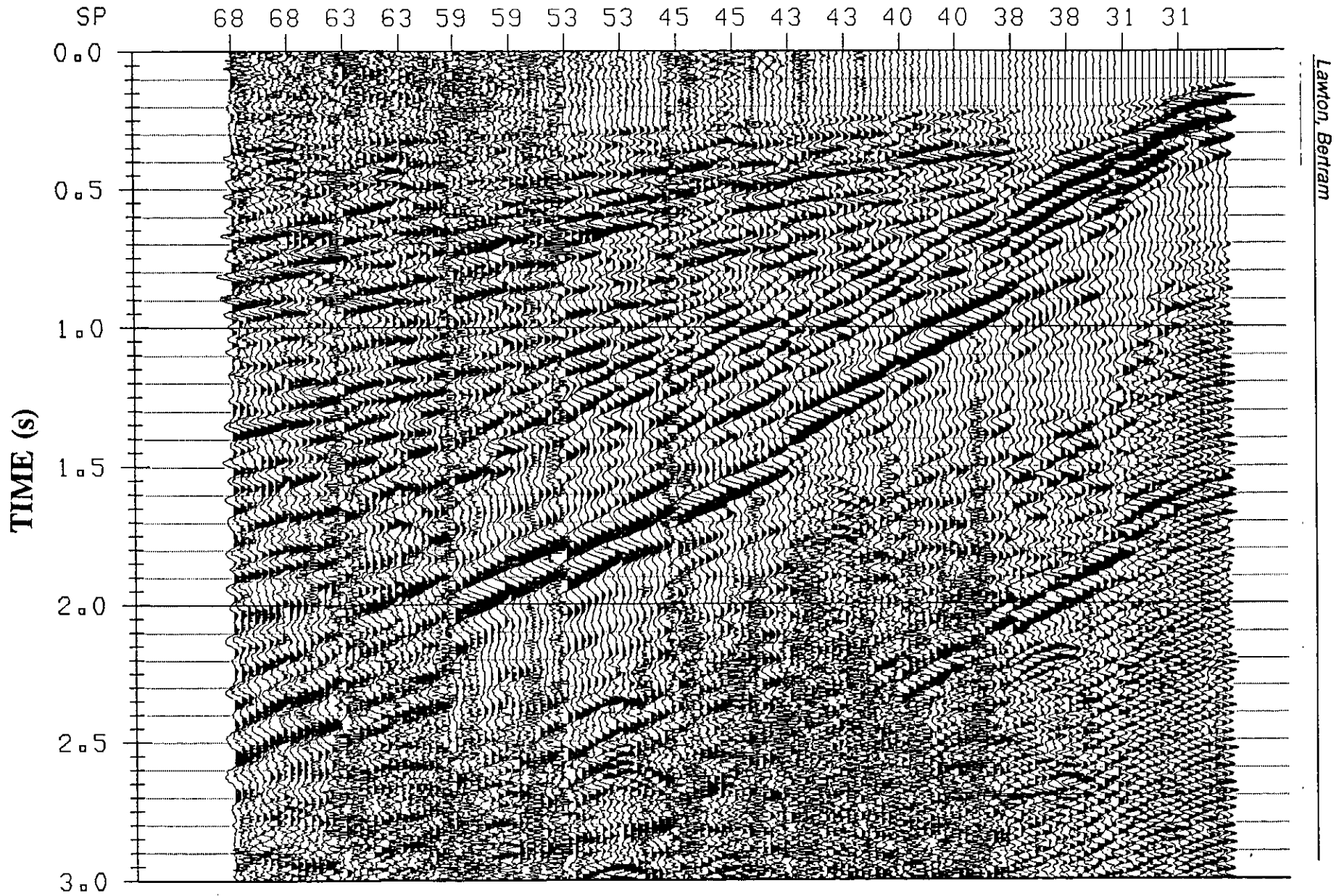


FIG. 5. P-T noise spread data, shotpoints 101 to 117 (every second trace)

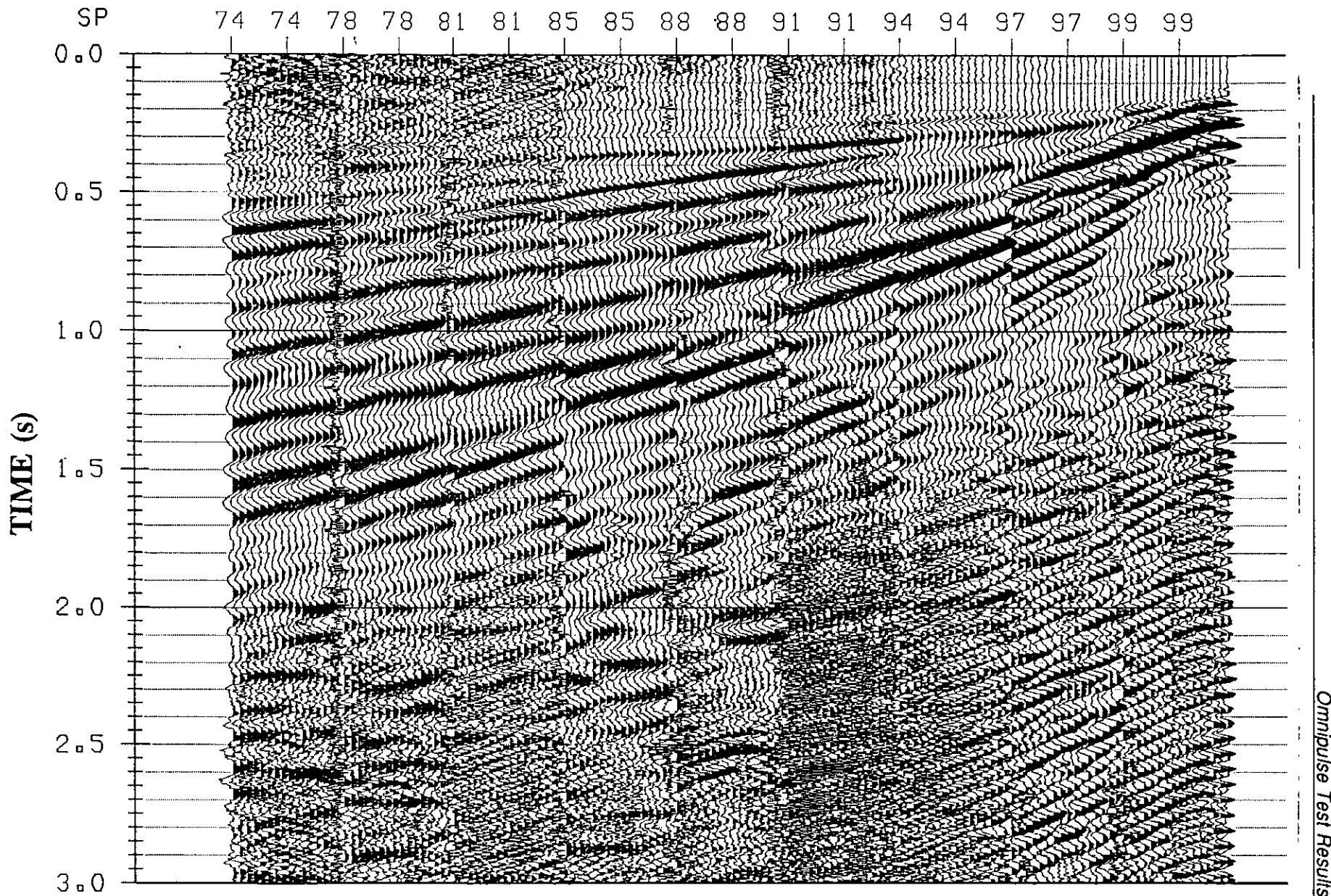


FIG 6. SV-V noise spread data, shotpoints 101 to 117 (every second trace)

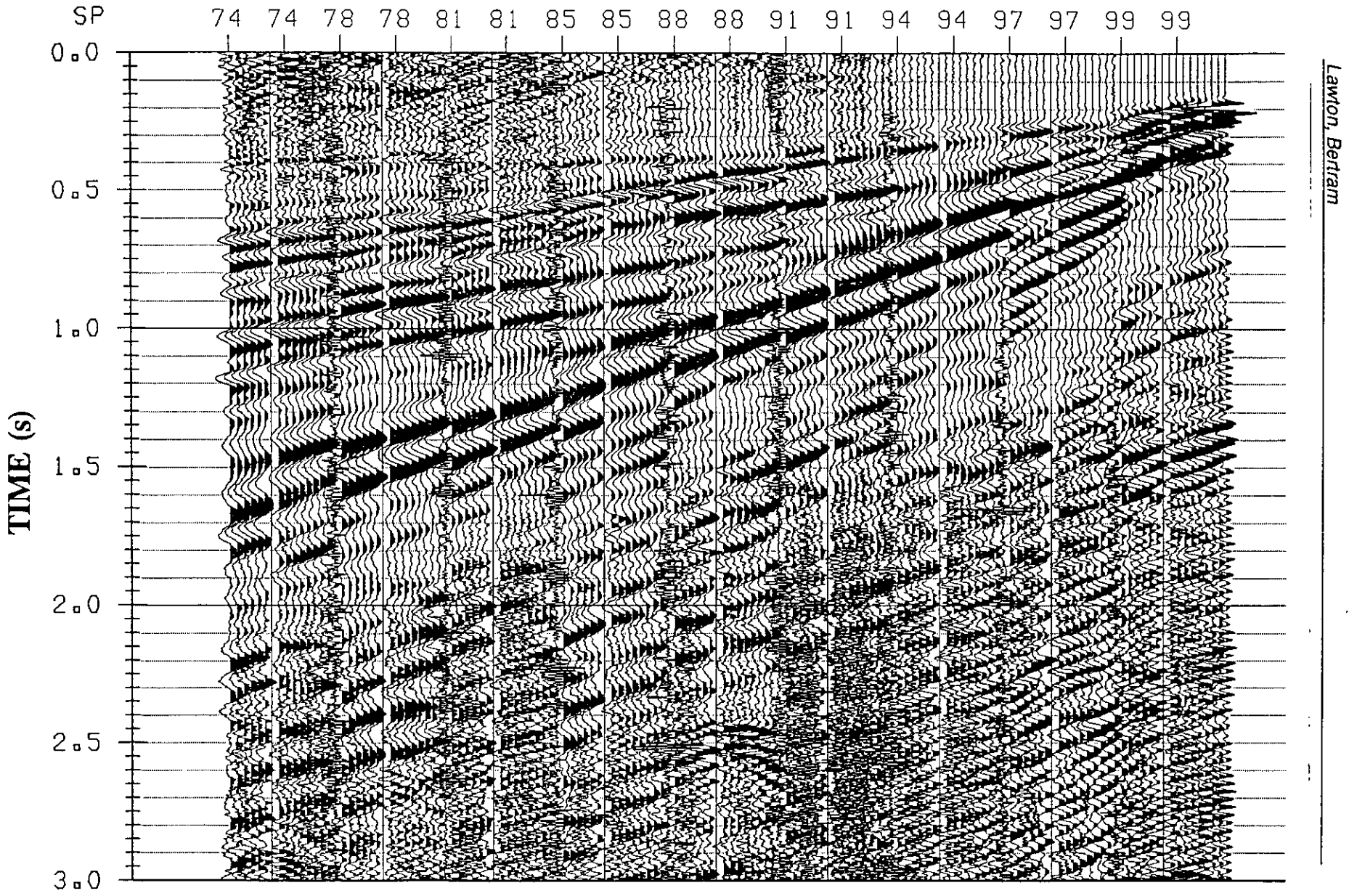


FIG. 7. SV-R noise spread data, shotpoints 101 to 117 (every second trace)

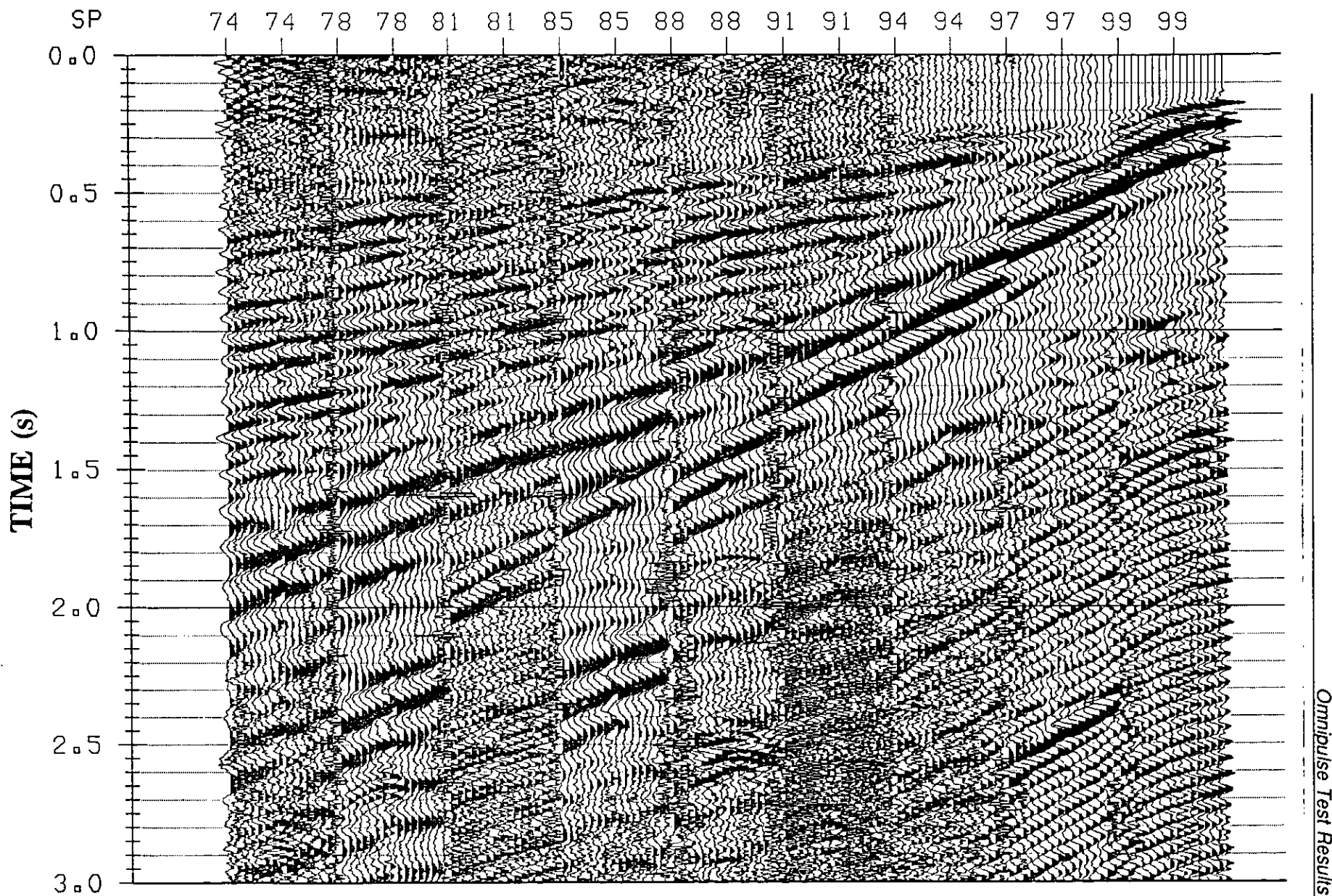


FIG. 8. SV-T noise spread data, shotpoints 101 to 117 (every second trace)

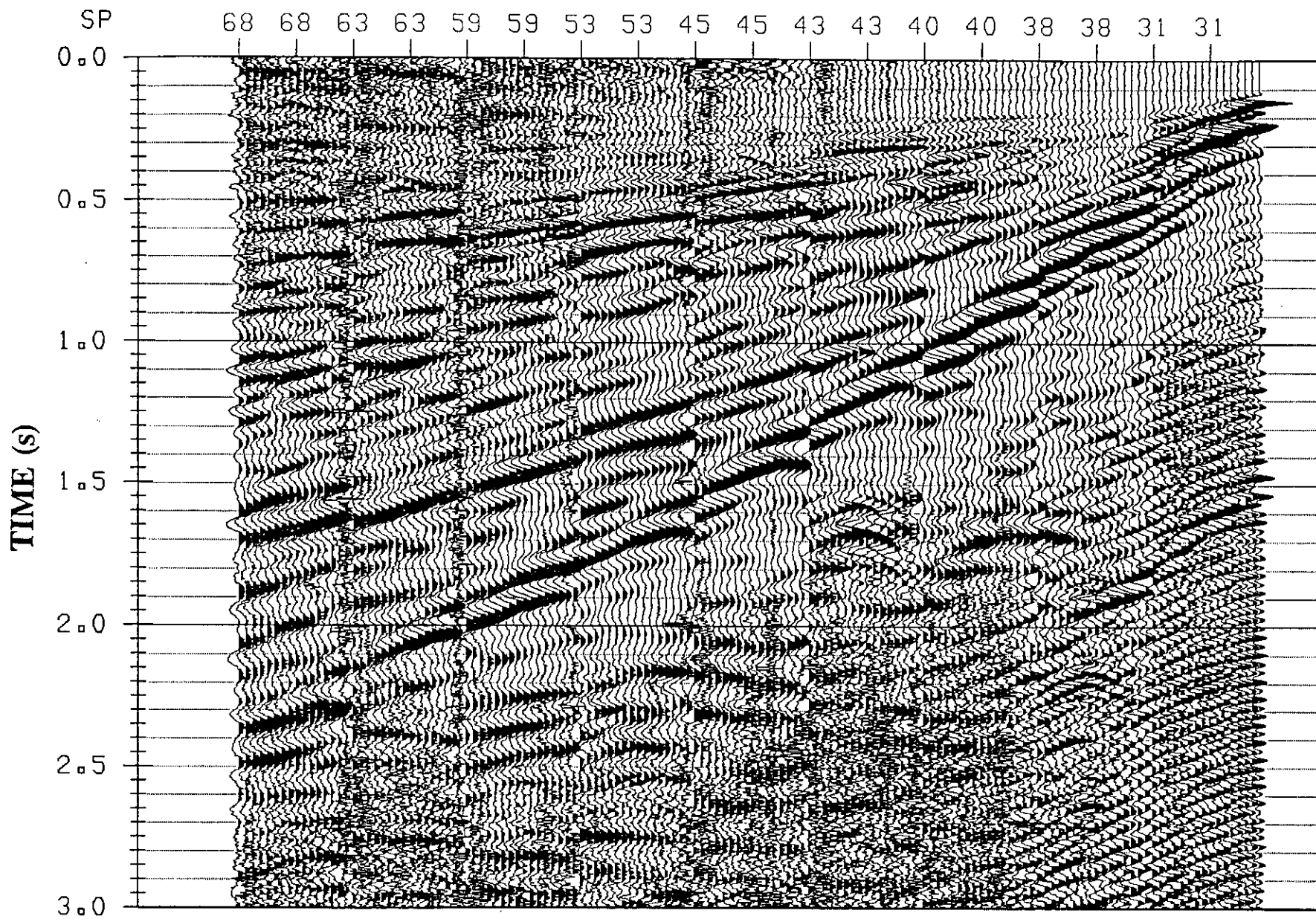


FIG. 9. SH-V noise spread data, shotpoints 101 to 117 (every second trace)

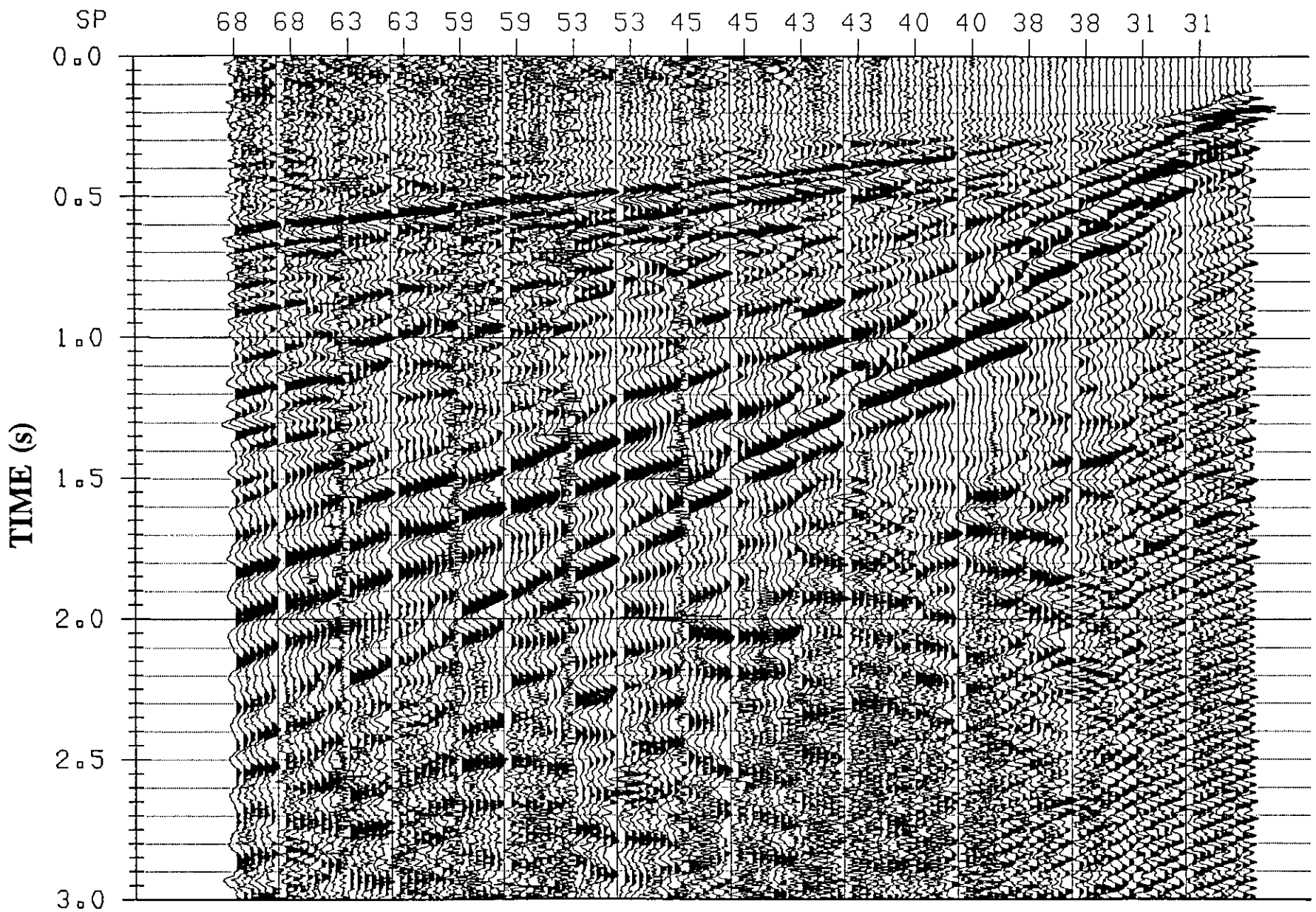


FIG. 10. SH-R noise spread data, shotpoints 101 to 117 (every second trace)

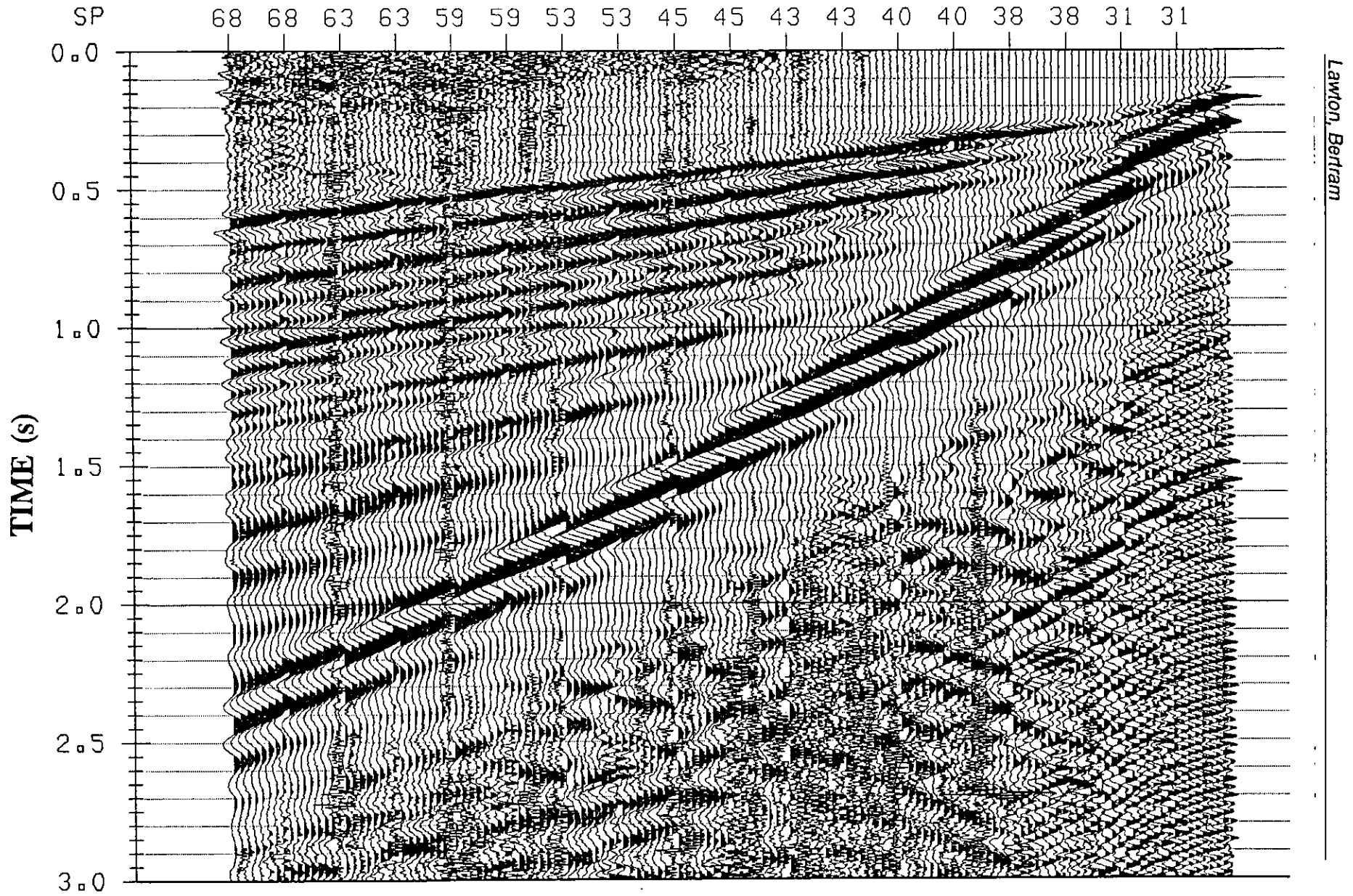


FIG. 11. SH-T noise spread data, shotpoints 101 to 117 (every second trace)

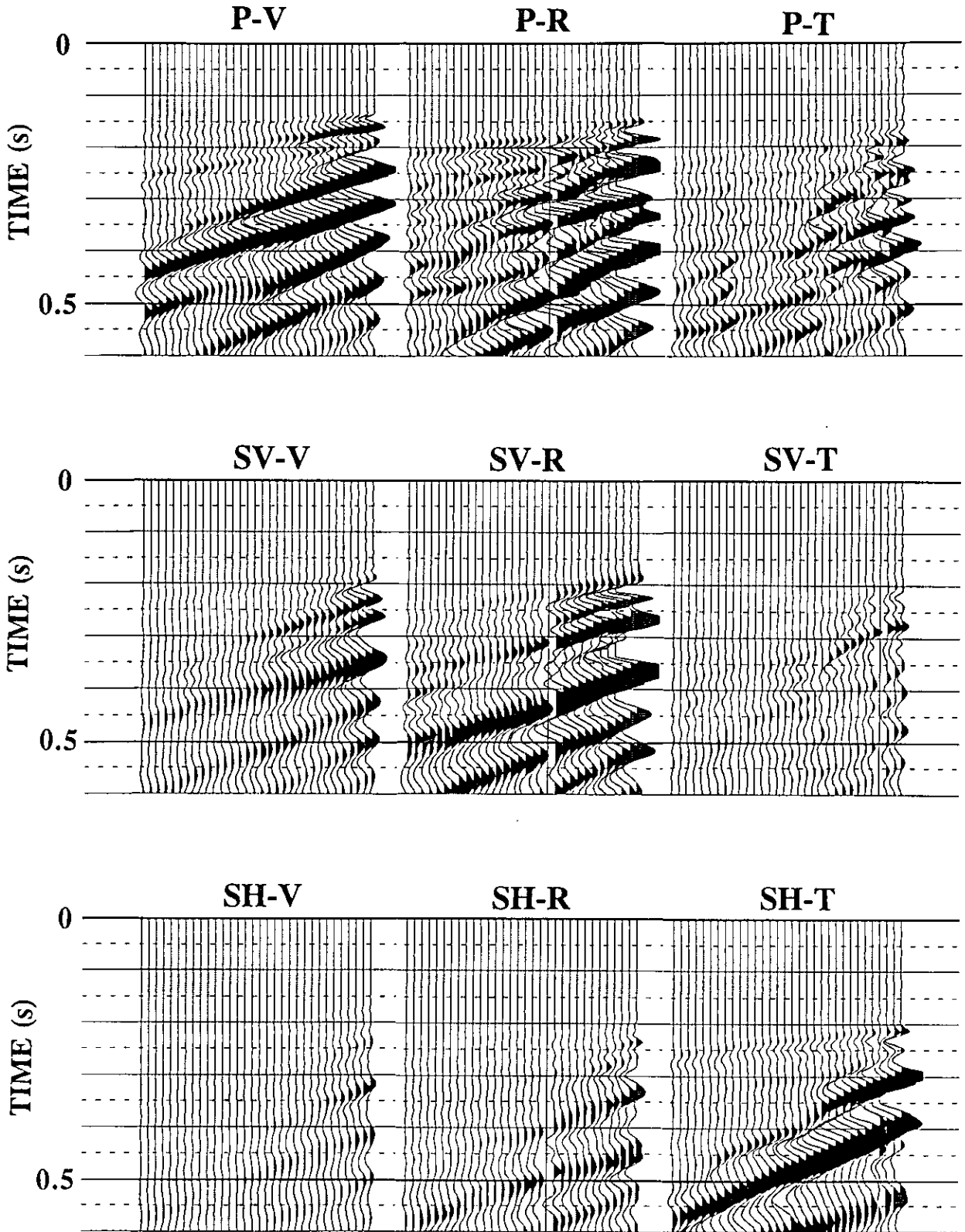


FIG. 12. Nine-component record from shotpoint N1. Traces have been plotted at true relative amplitude

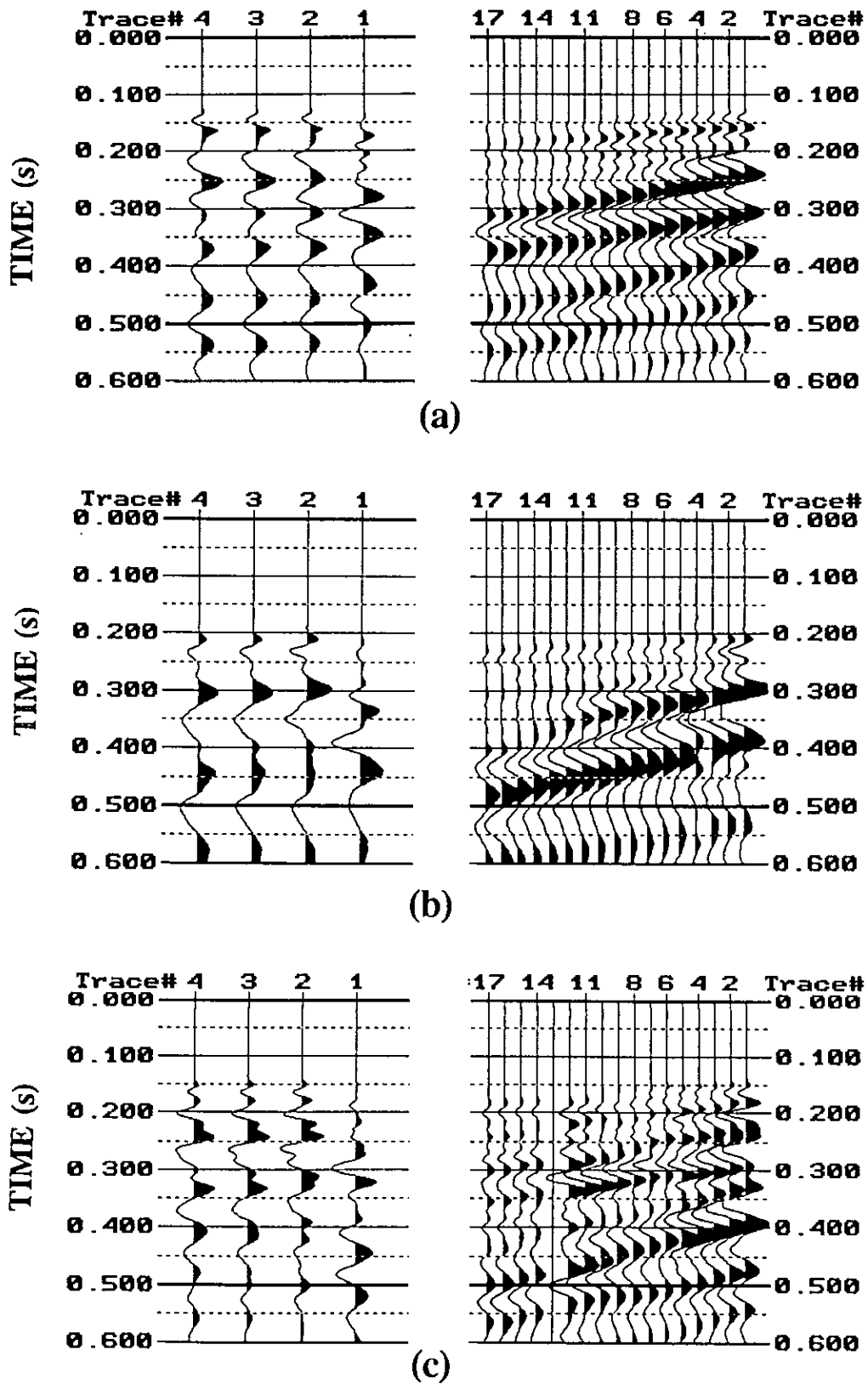
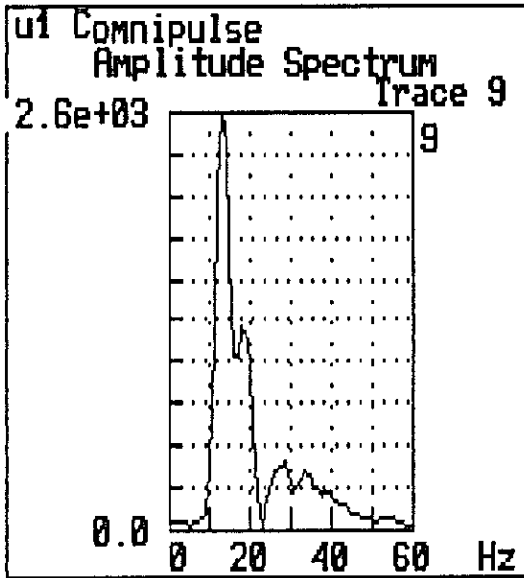
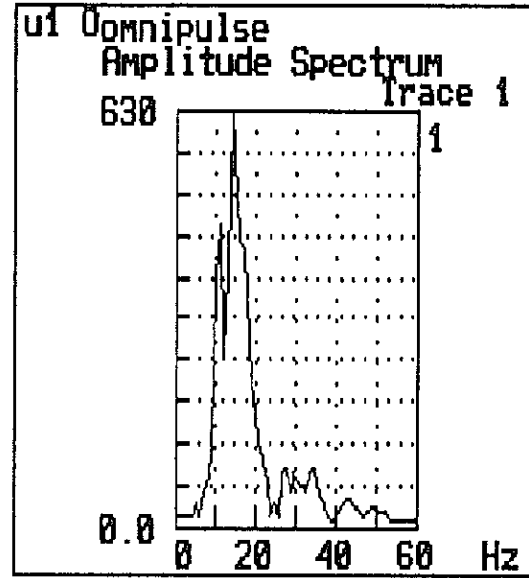


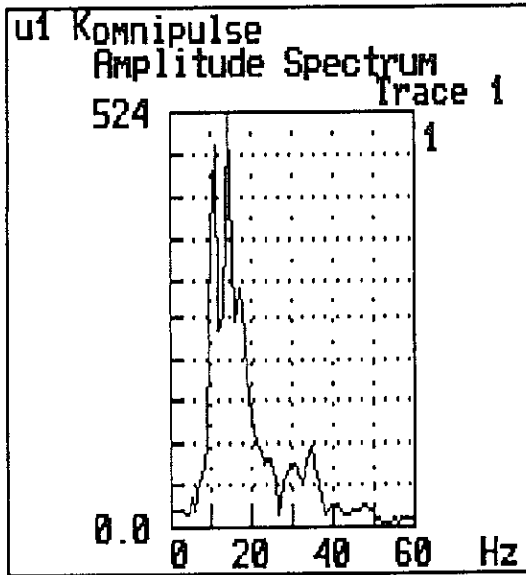
FIG. 13. Results of array-forming; (a) P-V record; (b) SH-T record; (c) P-R record. Raw records are displayed in the right hand panels. In the left panels, trace #1 is trace #9 of the raw data (centre trace), trace #2 is every fourth trace stacked, trace #3 is every second trace stacked and trace #4 is a stack of all traces.



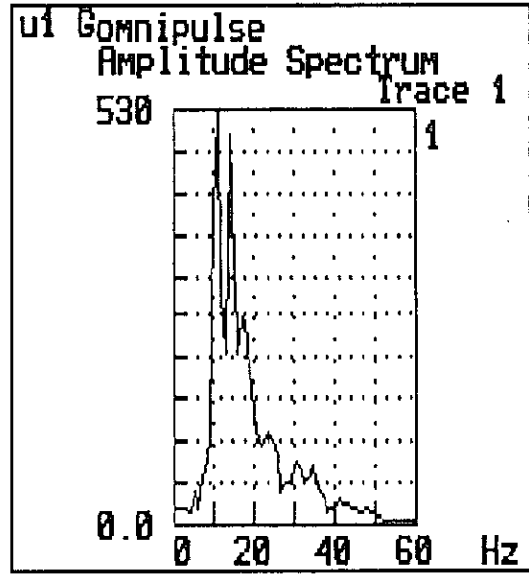
(a)



(b)

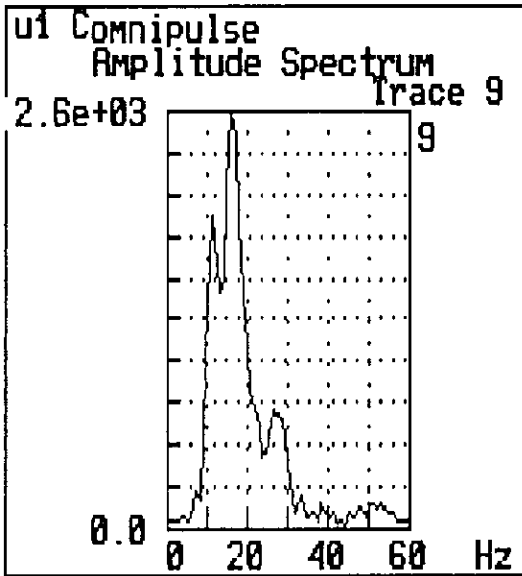


(c)

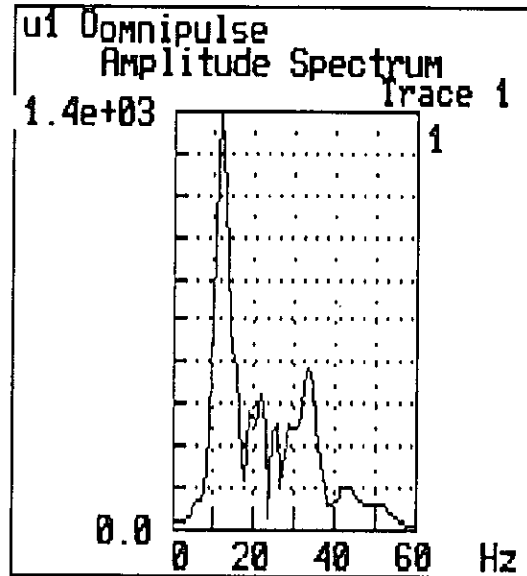


(d)

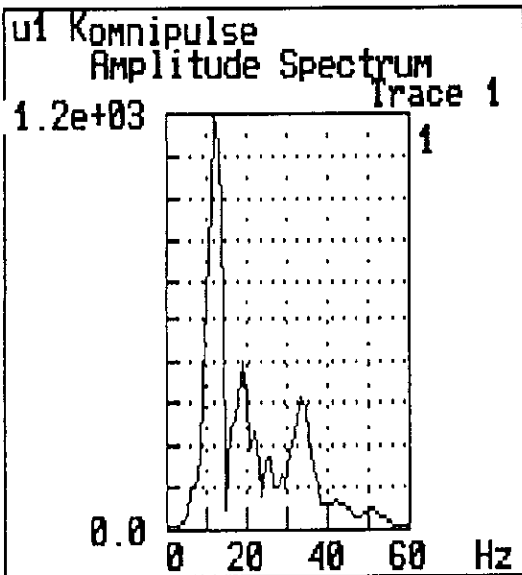
FIG. 14. Amplitude spectra of P-V stacked traces from Figure 13; (a) trace #1; (b) trace #2; (c) trace #4; (d) trace #3.



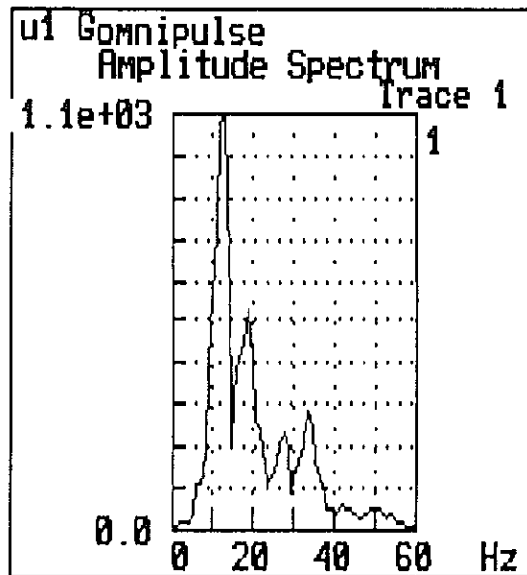
(a)



(b)

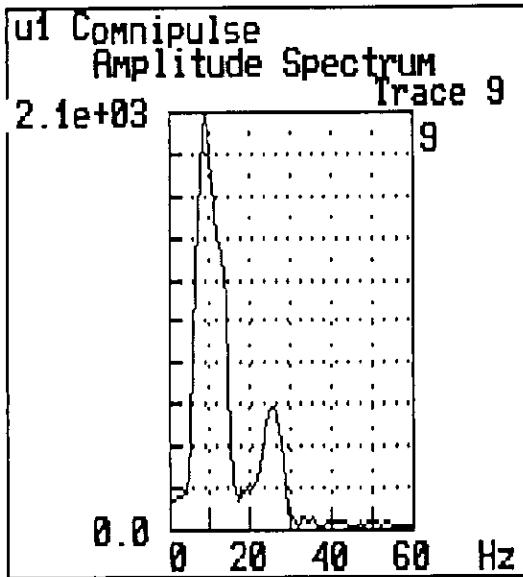


(c)

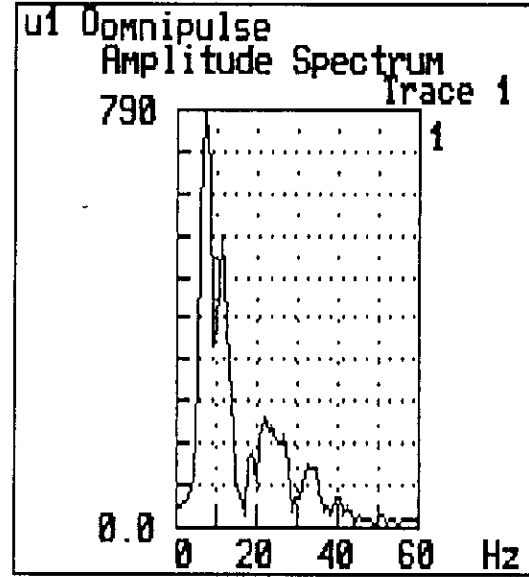


(d)

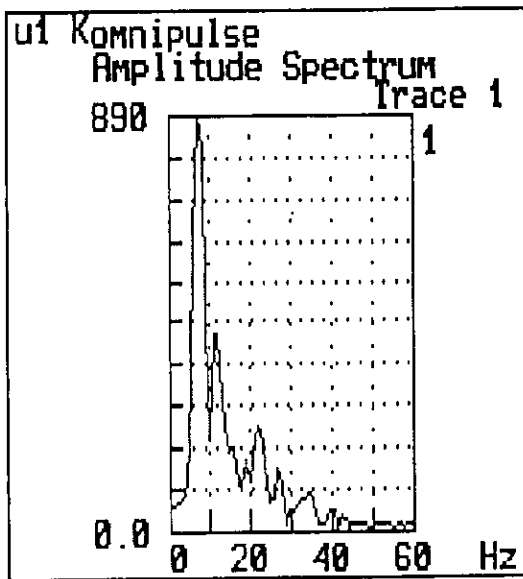
FIG. 15. Amplitude spectra of SH-T stacked traces from Figure 13; (a) trace #1; (b) trace #2; (c) trace #4; (d) trace #3.



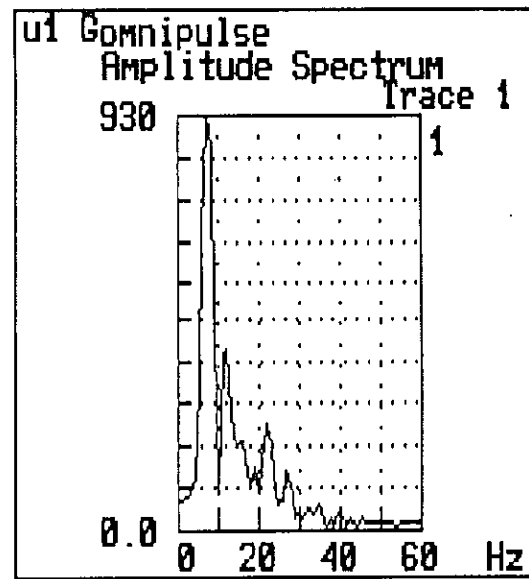
(a)



(b)



(c)



(d)

FIG. 16. Amplitude spectra of P-R stacked traces from Figure 13; (a) trace #1; (b) trace #2; (c) trace #4; (d) trace #3.

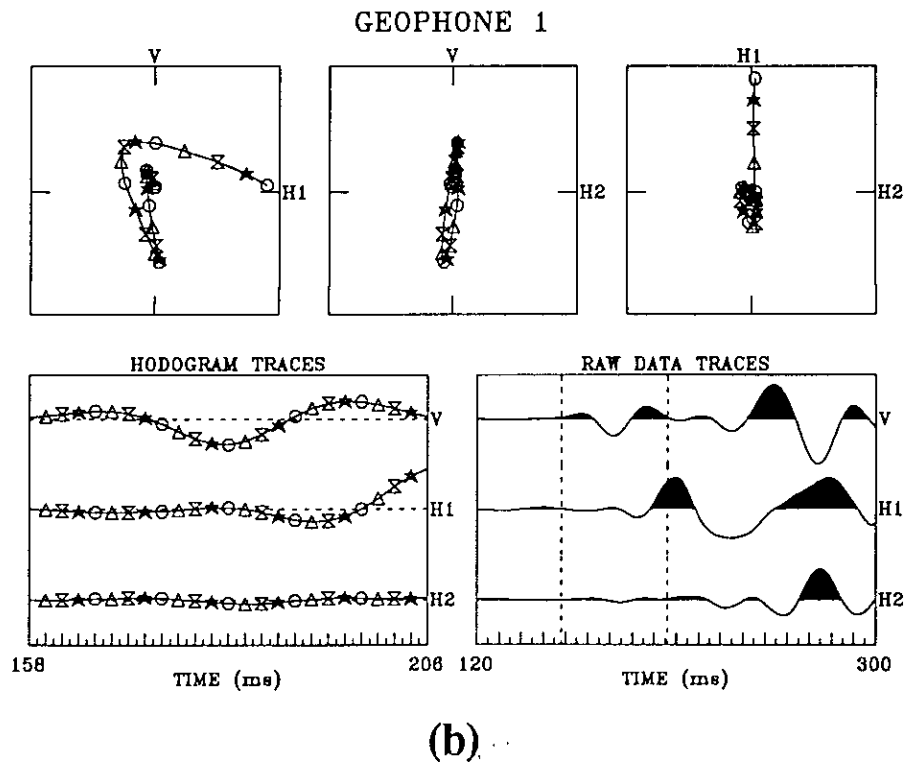
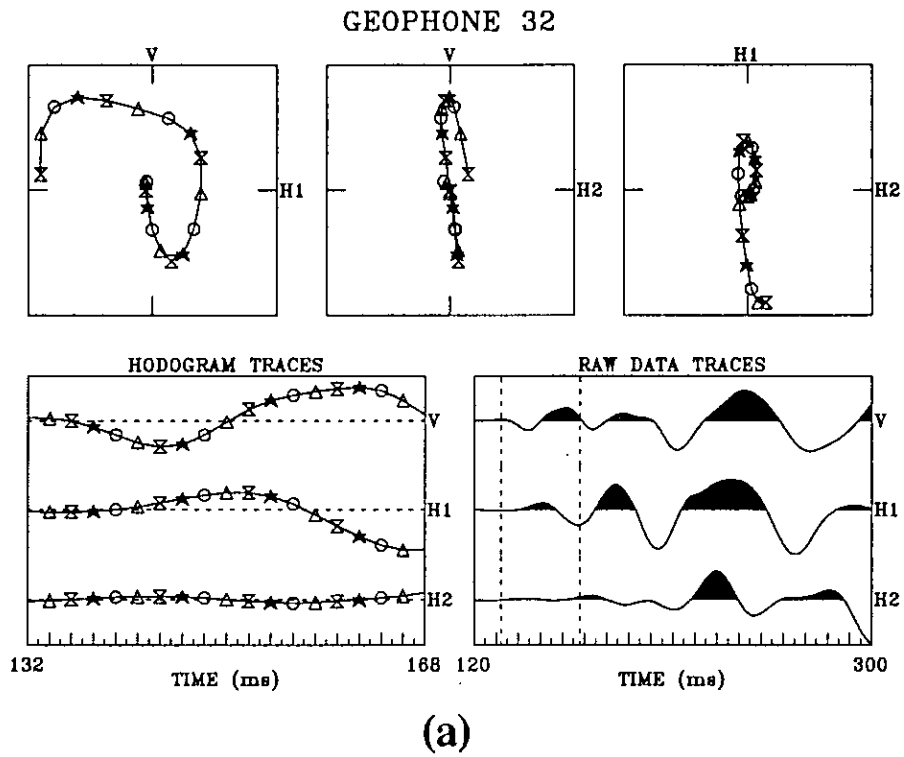


FIG. 17. Hodogram display of SV record from shotpoint N1; (a) geophone #32 (near traces); (b) geophone #1 (far traces).

APPENDIX

Omnipulse source azimuth and offset data

Rec ===	Shot ====	Azimuth =====	Distance =====	Rec ===	Shot ====	Azimuth =====	Distance =====
G32	83	357.78	482.1	G32	109	184.00	300.7
GC	83	357.91	512.0	GC	109	184.45	270.8
G1	83	358.02	542.0	G1	109	185.00	240.9
G32	85	356.02	421.0	G32	111	183.34	360.6
GC	85	356.29	450.9	GC	111	183.64	330.7
G1	85	356.52	480.9	G1	111	184.00	300.7
G32	87	353.55	368.3	G32	113	182.86	420.5
GC	87	354.03	398.2	GC	113	183.08	390.6
G1	87	354.45	428.0	G1	113	183.34	360.6
G32	89	351.10	307.2	G32	115	182.51	480.5
GC	89	351.89	336.9	GC	115	182.67	450.5
G1	89	352.56	366.6	G1	115	182.86	420.5
G32	91	348.28	246.1	G32	117	182.23	540.4
GC	91	349.55	275.6	GC	117	182.36	510.4
G1	91	350.57	305.1	G1	117	182.51	480.5
G32	93	347.29	194.1	G32	C1	0.00	169.7
GC	93	348.98	223.4	GC	C1	0.00	199.7
G1	93	350.28	252.9	G1	C1	0.00	229.7
G32	95	338.44	130.1	G32	C2	53.09	182.5
GC	95	342.43	158.4	GC	C2	46.26	201.9
G1	95	345.21	187.2	G1	C2	40.70	223.7
G32	97	329.91	72.8	G32	C3	98.42	204.9
GC	97	338.57	99.9	GC	C3	90.00	202.7
G1	97	343.47	128.3	G1	C3	81.58	204.9
G32	99	273.54	21.0	G32	C4	138.68	214.6
GC	99	326.14	37.7	GC	C4	132.80	193.1
G1	99	341.09	64.8	G1	C4	125.53	174.1
G32	100	210.26	34.7	G32	C5	180.00	230.0
GC	100	270.00	17.5	GC	C5	180.00	200.0
G1	100	329.74	34.7	G1	C5	180.00	170.0
G32	101	196.26	62.5	G32	C6	219.60	225.3
GC	101	210.26	34.7	GC	C6	225.00	203.1
G1	101	270.00	17.5	G1	C6	231.65	183.1
G32	103	189.46	121.7	G32	C7	261.29	198.2
GC	103	192.53	92.2	GC	C7	270.00	195.9
G1	103	198.43	63.2	G1	C7	278.71	198.2
G32	105	186.62	181.2	G32	C8	308.33	182.7
GC	105	187.93	151.4	GC	C8	315.00	202.7
G1	105	189.88	121.8	G1	C8	320.41	224.9
G32	107	185.00	240.9	G32	N1	0.00	30.0
GC	107	185.71	211.0	GC	N1	0.00	60.0
G1	107	186.65	181.2	G1	N1	0.00	90.0
				G32	S1	180.00	90.0
				GC	S1	180.00	60.0
				G1	S1	180.00	30.0